Cerebellum (2014) 13:29–41
DOI 10.1007/s12311-013-0516-5

ORIGINAL PAPER

Mutant Ataxin-3 with an Abnormally Expanded Polyglutamine Chain Disrupts Dendritic Development and Metabotropic Glutamate Receptor Signaling in Mouse Cerebellar Purkinje Cells

Ayumu Konno · Anton N. Shuvaev · Noriko Miyake · Koichi Miyake · Akira Iizuka · Serina Matsuura · Fathul Huda · Kazuhiro Nakamura · Shigeru Yanagi · Takashi Shimada · Hirokazu Hirai

Published online: 20 August 2013
© Springer Science+Business Media New York 2013

Abstract Spinocerebellar ataxia type 3 (SCA3) is caused by the abnormal expansion of CAG repeats within the ataxin-3 gene. Previously, we generated transgenic mice (SCA3 mice) that express a truncated form of ataxin-3 containing abnormally expanded CAG repeats specifically in cerebellar Purkinje cells (PCs). Here, we further characterize these SCA3 mice. Whole-cell patch-clamp analysis of PCs from advanced-stage SCA3 mice revealed a significant decrease in membrane capacitance due to poor dendritic arborization and the complete absence of metabotropic glutamate receptor subtype1 (mGluR1)-mediated retrograde suppression of synaptic transmission at parallel fiber terminals, with an overall preservation of AMPA receptor-mediated fast synaptic transmission. Because these cerebellar phenotypes are reminiscent of retinoic acid receptor-related orphan receptor α (RORα)-defective *staggerer* mice, we examined the levels of RORα in the SCA3 mouse cerebellum by immunohistochemistry and found a marked reduction of RORα in the nuclei of SCA3 mouse PCs. To confirm that the defects in SCA3 mice were caused by postnatal deposition of mutant ataxin-3 in PCs, not by genome disruption via transgene insertion, we tried to reduce the accumulation of mutant ataxin-3 in developing PCs by viral vector-mediated expression of CRAG, a molecule that facilitates the degradation of stress proteins. Concomitant with the removal of mutant ataxin-3, CRAG-expressing PCs had greater numbers of differentiated dendrites compared to non-transduced PCs and exhibited retrograde suppression of synaptic transmission following mGluR1 activation. These results suggest that postnatal nuclear accumulation of mutant ataxin-3 disrupts dendritic differentiation and mGluR-signaling in SCA3 mouse PCs, and this disruption may be caused by a defect in a RORα-driven transcription pathway.

Keywords Purkinje cell · Metabotropic glutamate receptor · Endocannabinoid · Spinocerebellar ataxia type 3 · Patch clamp

Ayumu Konno and Anton N. Shuvaev contributed equally to this work.

Electronic supplementary material The online version of this article (doi:10.1007/s12311-013-0516-5) contains supplementary material, which is available to authorized users.

A. Konno · A. N. Shuvaev · A. Iizuka · S. Matsuura · F. Huda · K. Nakamura · H. Hirai (✉)
Department of Neurophysiology, Gunma University Graduate School of Medicine, Maebashi, Gunma 371-8511, Japan
e-mail: hirai@gunma-u.ac.jp

A. N. Shuvaev
Department of Neurosurgery and Neurology, Krasnoyarsk State Medical University, Krasnoyarsk 660022, Russia

N. Miyake · K. Miyake · T. Shimada
Department of Biochemistry and Molecular Biology, Nippon Medical School, Tokyo 113-8602, Japan

S. Yanagi
Laboratory of Molecular Biochemistry, Graduate School of Life Sciences, Tokyo University of Pharmacy and Life Sciences, Tokyo, Japan

Introduction

Spinocerebellar ataxia (SCA) is a neurodegenerative disease that generally affects a wide range of areas in the central nervous system (CNS) including the cerebellum, brain stem, and spinal cord. About one third of the cases of SCA in patients are hereditary, in which polyglutamine (polyQ) diseases are most frequently observed. PolyQ diseases are caused

by an abnormal expansion of the CAG trinucleotide repeat within a coding region of a gene [1]. SCA type 3 (SCA3), also known as Machado–Joseph disease, is the most frequently observed polyQ disease and is caused by a CAG repeat expansion within the coding region of the ataxin-3 gene [2].

Previously, we generated SCA3 model mice (SCA3 mice) that express N-terminally truncated ataxin-3 with an abnormally expanded polyQ stretch specifically within cerebellar Purkinje cells (PCs). These SCA3 mice show polyQ aggregates in the nuclei of PCs in addition to impaired PC dendritic differentiation, which result in a markedly atrophied cerebellum and severe ataxia [3]. We succeeded in removing the polyQ depositions from affected PCs and consequently significantly rescued SCA3 mice from ataxia through the cerebellar injection of lentiviral vectors expressing CRAG (collapsin response mediator protein-associated molecule-associated guanosine triphosphatase), a molecule that facilitates the ubiquitin proteasome pathway [4]. However, how the mutant ataxin-3 with abnormally expanded polyQ affects PC function remained to be examined. In this study, we characterized the electrophysiological and morphological abnormalities of mature SCA3 mice to clarify the pathology of mutant ataxin-3 in PCs.

Material and Methods

Animals

C57BL/6 SCA3 mice expressing an N-terminal-truncated ataxin-3 gene with 69 CAG repeats [3, 5] and their wild-type littermates were used in this study. Animals were maintained on a 12-h light/dark cycle with free access to food and water. All animal experiments were approved by the Gunma University Animal Care and Experimental Committee and were conducted in accordance with the institutional and national guide for the care and use laboratory animals.

Electrophysiology Assay

Parasagittal cerebellar slices (200 μm in thickness) were prepared, and whole-cell recordings were conducted as previously described [6, 7]. Briefly, mice were deeply anesthetized using isoflurane (3 %) and were then euthanized. The entire brain was quickly removed and immersed for several minutes in an ice-cold solution containing (in millimolars) 234 sucrose, 26 $NaHCO_3$, 2.5 KCl, 1.25 NaH_2PO_4, 11 D-glucose, 10 $MgSO_4$, and 0.5 $CaCl_2$ (pH 7.4, bubbled with 95 % O_2 and 5 % CO_2). Parasagittal slices of the cerebellar vermis were obtained using a microslicer (ZERO1; Dosaka-EM, Kyoto, Japan). The slices were maintained in an extracellular solution containing (in millimolars) 125 NaCl, 2.5 KCl, 2 $CaCl_2$, 1 $MgCl_2$, 1.25 NaH_2PO_4, 26 $NaHCO_3$, 10 D-glucose, and 0.1 picrotoxin. The solution was bubbled continuously with a mixture of 95 % O_2 and 5 % CO_2 at room temperature for at least 45 min prior to initiating the recordings. Whole-cell voltage-clamp recordings were made using an intracellular solution containing (in millimolars) 65 K-gluconate, 65 Cs-methanesulfonate, 10 KCl, 1 $MgCl_2$, 4 Na_2ATP, 1 NaGTP, 20 HEPES, 0.4 EGTA, and 5 sucrose (pH 7.3, adjusted with CsOH). PCs were voltage-clamped at −70 mV to record parallel fiber (PF) EPSCs (excitatory postsynaptic currents) and at −10 mV to record climbing fiber (CF) EPSCs. The selective stimulation of CFs and PFs was confirmed by paired-pulse depression and paired-pulse facilitation of EPSC amplitudes, respectively, with a 50-ms interstimulus interval. Passive membrane properties such as the membrane capacitance (Cm) and membrane resistance (Rm) were obtained by applying hyperpolarizing voltage steps from −70 to −80 mV for 500 ms. PF- and CF-excitatory postsynaptic currents (EPSCs) were recorded from PCs voltage-clamped at −70 mV by electrical stimulation to PFs or CFs. Decay time constants for CF and PF EPSCs were measured by fitting the EPSC decay with a single exponential.

Endocannabinoid-mediated short-term depression of PF–PC synaptic transmission was examined using a Cs-based intracellular solution (in millimolars): 140 Cs-gluconate, 8 KCl, 10 HEPES, 1 $MgCl_2$, 2 MgATP, 0.4 NaGTP, and 0.2 EGTA. PF EPSCs were recorded from PCs voltage-clamped at −70 mV at a frequency of 0.2 Hz for 1 min. For the synaptically evoked suppression of excitation (SSE), the stable basal EPSC response was recorded for 1 min, and then a high-frequency PF stimulation (PF burst, 50 pulses at 100 Hz) was applied to activate the mGluR-mediated signaling cascade. To evoke the depolarization-induced suppression of excitation (DSE), a depolarizing pulse from −70 to 0 mV was applied to PCs for 5 s. To stimulate a similar number of PFs in each experiment, we adjusted the amplitude of PF EPSCs to approximately 400 pA (397.0±53.8 pA for wild-type mice PCs and 426.3±99.7 pA for SCA3 mice PCs) before the induction of SSE or DSE. PF EPSCs were recorded for 100 s after the stimulation. To verify that the observed suppression of PF EPSC amplitude was mediated by endocannabinoid signaling, the same experiments were conducted in the presence of AM251 (Tocris Bioscience, Ellisville, MO, USA), a CB1 receptor antagonist, at a concentration of 5 μM.

For the current-clamp experiments, the pipette solution was a K-gluconate-based intracellular solution containing (in millimolars) 130 K-gluconate, 4 KCl, 20 HEPES, 1 $MgCl_2$, 4 MgATP, 1 NaGTP, and 0.4 EGTA. Initially, the passive membrane properties of a PC voltage-clamped at −70 mV were recorded. The recording was then changed to current-clamp mode, and a depolarizing step current ranging from 0 to + 600 pA in increments of 50 pA with a step interval of 10 s was applied to the recording PC for a duration of 1 s.

Biocytin Infusion and Morphological Analysis

To visualize the morphology of PCs, 0.5 % biocytin (Sigma-Aldrich, St. Louis, MO, USA) diluted in the intracellular solution was infused by passive diffusion through a patch pipette into whole-cell-clamped PCs. Cerebellar slices were subsequently fixed with 4 % paraformaldehyde. Following an overnight fixation at 4 °C, the slices were rinsed in 0.1 M phosphate-buffered saline (PBS; pH 7.4) (3 times, 5 min each) and treated with PBS containing a streptavidin-Alexa 594 conjugate. After a 2-h incubation at room temperature, the slices were mounted with ProLong Gold Antifade Reagent (Life Technologies, Grand Island, NY, USA). The slices were then analyzed using a confocal laser-scanning microscope (LSM 5 PASCAL, Carl Zeiss, Oberkochen, Germany). For the confocal microscopic analysis, cerebellar slices were scanned at 1-μm intervals in Z-stack mode to project the entire dendritic tree onto a planar image.

Immunohistochemistry

Deeply anesthetized mice aged 14 weeks were perfused intracardially with 4 % paraformaldehyde in 0.1 M PBS (pH 7.4). The entire brain was removed and immersed in 4 % paraformaldehyde in 0.1 M PBS overnight at 4 °C. Parasagittal cerebellar slices (50 μm thick) were prepared using a vibratome (VT1000S, Leica, Wetzlar, Germany). These slices were permeabilized and blocked with PBS containing 2 % (*v*/*v*) normal donkey serum, 0.1 % (*v*/*v*) Triton X-100, and 0.05 % NaN_3 (blocking solution) and treated overnight with the following antibodies: rabbit polyclonal anti-mGluR1 (1:300, Frontier Institute, Ishikari, Japan), goat polyclonal anti-retinoic acid receptor-related orphan receptor α (RORα) (1:400, Santa Cruz Biotechnology, CA, USA), mouse monoclonal anti-calbindin D-28 k (1:1,000, Swant, Bellinzona, Switzerland), rabbit polyclonal anti-GFP (1:1,000; Frontier Institute), or rat monoclonal anti-HA (1:1,000; clone 3F10; Roche, Mannheim, Germany) in blocking solution. After washing four times with 0.1 % Triton X-100 (washing solution) at room temperature in PBS, the slices were treated with secondary antibodies in blocking solution. Alexa Fluor 488-conjugated donkey anti-rabbit IgG (1:1,000; Life Technologies), Alexa Fluor 568-conjugated donkey anti-rat IgG (1:1,000; Life Technologies), Alexa Fluor 568-conjugated donkey anti-goat IgG (1:1,000, Life Technologies), or Alexa Fluor 680-conjugated donkey anti-mouse IgG (1:1,000, Life Technologies) were used as secondary antibodies. Finally, the slices were washed four times in washing solution at room temperature and were mounted on glass slides with ProLong Gold Antifade Reagent (Life Technologies). Each specimen was observed under an inverted fluorescence microscope (DMI6000B, Leica) or a confocal laser-scanning microscope (LSM 5 PASCAL, Carl Zeiss). The fluorescent areas that were immunoreactive to HA were measured using WinROOF image analysis software (Mitani Corporation, Tokyo, Japan).

Production of AAV Vectors

N-terminal truncated ataxin-3 with an abnormally expanded polyQ repeat was specifically expressed in cerebellar PCs by PC-specific L7 promoter [5]. To express a therapeutic gene in PCs using adeno-associated viral vector serotype-9 (AAV9), we used the murine stem cell virus (MSCV) promoter, which possesses strong transcriptional activity in PCs [8]. The expression plasmid pAAV/MSCV-GFP-P2A-CRAG was obtained via enzymatic reactions using pNAV [9] and pCL20c/MSCV-GFP-P2A-CRAG [3]. Initially, pAAV/MSCV was generated by the insertion of the MSCV promoter fragment with blunted-*Mlu*I and *Bam*HI sites into blunted-*Xho*I and *Bam*HI sites of pNAV. Subsequently, the GFP-P2A-CRAG cassette with blunted-*Not*I and *Bam*HI sites was subcloned into pAAV/MSCV with blunted-*Eco*RI and *Bam*HI sites.

Recombinant single-strand AAV9 vectors were generated by the cotransfection of HEK293 cells with three plasmids, pAAV/MSCV-GFP-P2A-CRAG, pHelper (Stratagene, La Jolla, CA, USA), and pAAV2/9 (kindly provided by Dr. J. Wilson). The viral particles were purified using ammonium sulfate precipitation and iodixanol continuous gradient centrifugation as described previously [10]. The genomic titer of the purified AAV9 vector as determined by real-time PCR was 9.9×10^{14} vector genomes/ml.

Jugular Vein Injection

The mouse pups that were given viral injections were obtained by crossing heterozygous SCA3 mice to wild-type mice. The pups received an injection of purified AAV9 solution through the external jugular vein using a 0.1-ml Hamilton syringe (Hamilton Company, Reno, NV, USA) with a 30-gauge needle (Becton Dickinson & Co, Franklin Lakes, NJ, USA) on postnatal day (P) 1 or 2. Three weeks after the injection, the genotypes of the mice (heterozygous or wild type) were determined by PCR using the specific primers 5′-ATGTACCCATACGATGTTCC-3′ (sense) and 5′-CTAGCGAGGGAATGAAGAAT-3′ (anti-sense). Non-injected heterozygous and wild-type mice were used as controls.

Statistical Analysis

The results are expressed as the mean±SEM unless otherwise specified, and *n* indicates the number of tested PCs. Statistical analyses of the groups with one independent and two dependent variables were performed using the polynomial regression method. Statistical analyses of differences between

groups were performed using an unpaired *t* test, a one-way analysis of variance (ANOVA) followed by Tukey's post hoc test, or a Mann–Whitney *U* test. A probability of 0.05 was considered to represent statistical significance.

Results

Decreased Membrane Capacitance in SCA3 Mouse PCs

The electrophysiological properties of PCs from 4-month-old SCA3 mice and age-matched control mice were analyzed by the slice patch-clamp technique. Passive membrane properties in response to a 10-mV depolarizing pulse for 100 ms showed a significantly smaller membrane capacitance (Cm) in SCA3-mouse PCs (174.2±12.6 pF, $n=27$ PCs from four mice) compared to wild-type-mouse PCs (808.8±20.1 pF, $n=24$ PCs from five mice) (Fig. 1a), suggesting a severe impairment in dendrite arborization in SCA3-mouse PCs. Other passive membrane properties such as membrane and access resistance did not differ significantly between genotypes (Supplementary Table 1). Immunolabeling of biocytin infused into PCs confirmed markedly poorer dendritic arborization in SCA3-mouse PCs compared to wild-type PCs (Fig. 1b).

An analysis of PF EPSC kinetics showed significantly faster rise and decay time constants in SCA3 mice than in wild-type littermates (Fig. 1c, d and Supplementary Table 1), which could be explained by the markedly affected dendritic development and therefore an electrically more compact morphology of SCA3 mouse PCs. There were no significant differences in the kinetics of CF-mediated EPSCs and short-term synaptic plasticity in response to paired pulse stimulation of PFs or CFs (Fig. 1c, d and Supplementary Table 1).

Impairment of Endocannabinoid-Mediated Presynaptic Inhibition in SCA3 Mouse PCs

A brief burst of PF stimulation in PCs causes the activation of mGluR1 and local elevation of Ca^{2+} due to AMPA receptor-mediated depolarization. These effects produce endocannabinoids and lead to the retrograde suppression of glutamate release from presynaptic PF terminals (synaptically evoked suppression of excitation, SSE) [11–14]. Therefore, we examined SSE to assess the function of mGluR1 in SCA3-mouse PCs. In response to tetanic stimulation, the amplitudes of PF EPSCs in control PCs from wild-type animals decreased to approximately 20 % of the prestimulation levels, and more than 60 s elapsed before the amplitudes returned to their original levels. In contrast, the amplitudes of PF EPSCs in SCA3-mouse PCs increased to approximately 140 % of the prestimulation levels (Fig. 2a). These results could be ascribed to an impairment of mGluR signaling in SCA3-mouse PCs.

In addition to the mGluR signaling pathway, SCA3 mouse PCs may also possess defects in the endocannabinoid-mediated signaling pathway, such as an alteration in endocannabinoid release from PCs. To test this possibility, we examined the

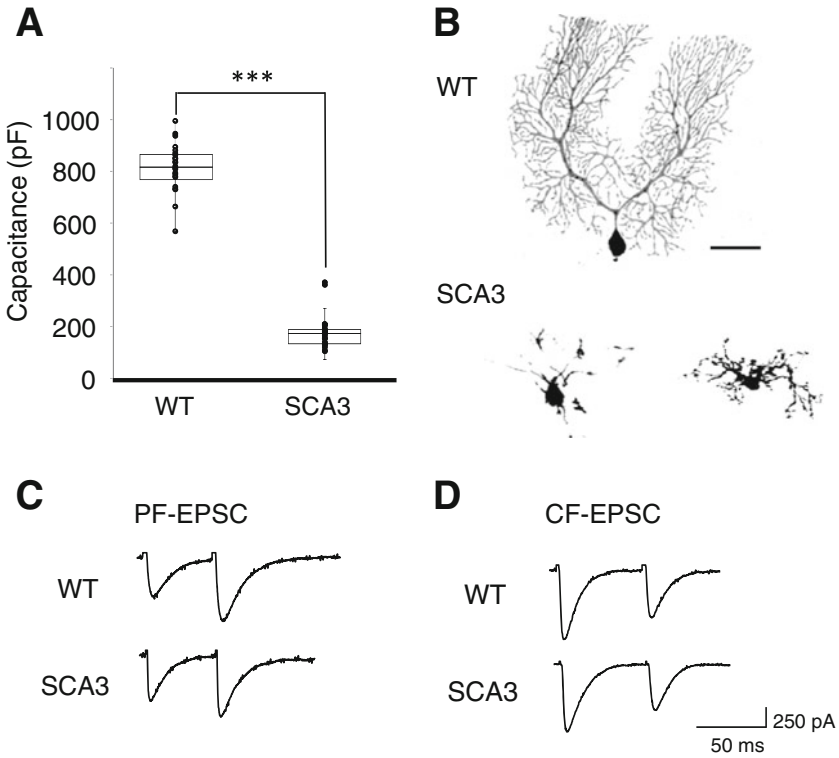

Fig. 1 Impaired dendrite arborization of heterozygous SCA3 mouse PCs at 13–16 weeks of age. **a** Membrane capacitance of PCs from wild-type (*WT*) and heterozygous SCA3 mice. Each *point in the graph* represents the membrane capacitance (pF) of a PC. *Boxes* and *error bars* show the standard error of mean values and standard deviation, respectively. The *middle lines in boxes* show the average value of each group. *Asterisks* indicate statistically significant differences as determined by an unpaired *t* test, ***$p<0.001$. **b** Representative images of biocytin-labeled PCs from wild-type and heterozygous SCA3 mice. *Scale bar*, 50 μm. **c**, **d** Representative traces of PF- (**c**) and CF-EPSC (**d**) from wild-type and heterozygous SCA3 mouse PCs

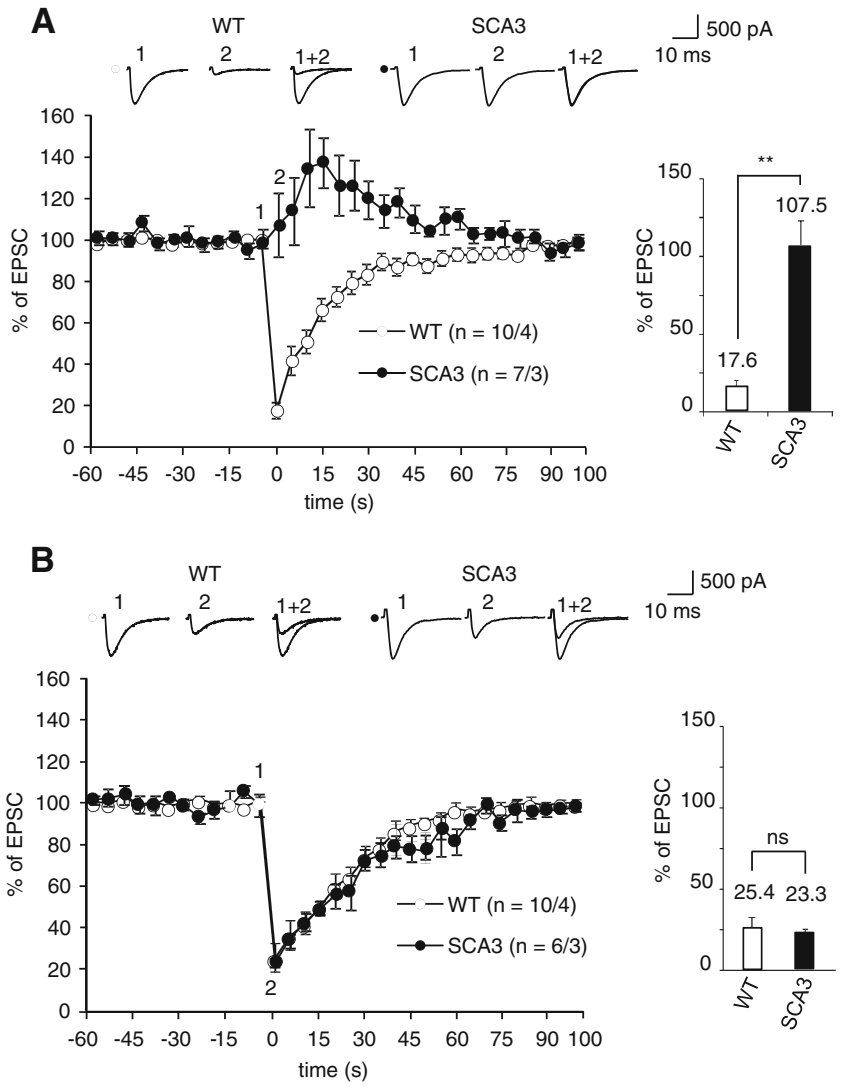

Fig. 2 Impairment of synaptically evoked suppression of excitation (SSE), but not depolarization-induced suppression of excitation (DSE), of PF EPSCs in 13–16-week-old SCA3 mouse PCs. The amplitude of PF EPSC was adjusted to approximately 400 pF before induction of SSE or DSE. The SSE was induced by a PF burst (50 pulses at 100 Hz), while DSE was evoked by depolarization of a PC from −70 to 0 mV for 5 s. **a** Time course of changes in the PF EPSC amplitude before and after the PF burst, showing a complete absence of SSE in SCA3-mouse PCs. The *right graph* shows the percentage of the EPSC amplitude just after the PF burst relative to the baseline value (*right*). **b** Time course of changes in the PF EPSC amplitude before and after 5-s depolarization of PCs, showing a reliable occurrence of DSE in both wild-type and SCA3-mouse PCs. The *right graph* shows the percentage of the EPSC amplitude just after the depolarization. The *inset traces* in **a** and **b** represent the last EPSC of the basal recordings (the EPSC just before the stimulation) (*1*) and the first EPSC after the PF burst in each experimental condition (*2*). The numbers (*n*) of tested PCs and animals (PCs/animals) are indicated on the *graph*. *Asterisks* indicate a statistically significant difference in comparison to wild-type mice, as determined by an unpaired *t* test, $^{**}p<0.01$

mGluR-independent form of endocannabinoid-mediated retrograde signaling (depolarization-induced suppression of excitation, DSE). In DSE, endocannabinoid release from PCs is driven solely by an exceptionally large increase in intracellular calcium (in the micromolar range), which is induced by depolarization and does not rely on the activation of mGluRs [15–18]. After PCs from SCA3 and wild-type mice were depolarized from −70 to 0 mV for 5 s, the subsequent initial PF EPSC amplitudes were reduced to approximately 20 % of the basal amplitude prior to depolarization, and they returned to basal levels 80 s after depolarization (Fig. 2b). There were no significant differences in the degree of DSE or the recovery time course between SCA3-mouse PCs and control PCs. However, the depression in the SCA3-mouse PCs may have been induced by mechanisms other than endocannabinoid signaling. To confirm that the depolarization-induced suppression of PF EPSCs observed in SCA3 mice was mediated by endocannabinoid signaling and not by some other mechanism, we conducted the same experiment in the presence of AM251, an antagonist of the presynaptic endocannabinoid CB1 receptor. Bath application of AM251 clearly abolished DSE in SCA3 mice (Supplementary figure 1), indicating that the DSE induced

in the SCA3-mouse cerebellum was primarily mediated by endocannabinoid signaling. Thus, we conclude that the observed impairment in SSE in SCA3-mouse PCs is due to defects in mGluR signaling rather than defects in endocannabinoid-mediated retrograde signaling.

Decreased Expression Levels of RORα in the Nuclei of SCA3-Mouse PCs

We have recently shown that homozygous *staggerer* mutant mice, which lack RORα protein, exhibit an impaired development of PC dendritic arborization, a disruption in the arrangement of PC soma in the PC layer, and a functional loss of mGluR signaling with relative preservation of fast synaptic transmission at PF–PC synapses [19]. All of these phenotypes were shared with the present SCA3 mice, although the phenotypes of SCA3 mice were less severe than those of *staggerer* mice (Supplementary figure 2). RORα is abundantly expressed in PCs and is a transcription factor that triggers the expression of various molecules including those involved in dendritic differentiation and glutamate signaling [20]. The *staggerer* mouse is a loss-of-function mutant caused by a 122-bp deletion of the *rora* gene [21], and they show a defect in RORα-mediated transcription.

To examine the pathological convergence of the SCA3 mouse with the *staggerer* mutants, the expression of RORα and mGluR1 protein in the SCA3-mouse cerebellum was examined by immunohistochemistry. High amounts of RORα were expressed in PC nuclei with modest levels of RORα expression in stellate and basket cells of wild-type mice (Fig. 3). In contrast, SCA3-mouse PCs exhibited markedly decreased levels of RORα although the amount of RORα in the interneurons was maintained or enhanced (Fig. 3b). Moreover, similar to homozygous *staggerer* mutant mice, mGluR1 protein, which is localized precisely in the dendritic spines opposing presynaptic PF terminals in the wild-type mouse PC (Fig. 3a), formed granular aggregates in the dendrites of SCA3 mouse PCs (Fig. 3b and Supplementary figure 2). These results suggest that a reduction in RORα within PC nuclei and the subsequent defects of RORα-driven transcription in SCA3 mice may underlie the aberrant phenotypes shared with the RORα-defective homozygous *staggerer* mice, such as the impaired development of PC dendrites, the disrupted arrangement of PC somata, and the loss of mGluR signaling.

Limited Expression of a Transgene by AAV9 Vectors in SCA3 Mouse Cerebellum

To confirm that the morphological and electrophysiological defects of SCA3 mice were caused by postnatal deposition of mutant ataxin-3, not by specific genome disruption via transgene insertion, we tried to reduce the amount of mutant ataxin-3 from PC nuclei by the AAV9-mediated expression of CRAG in PCs. AAV9 expressing CRAG together with GFP was administered to SCA3 mice and their wild-type littermates at P 1 or 2 through the jugular vein. The expression of the transgene in the cerebellum was examined 14 weeks after the viral injection. Figure 4 shows representative sagittal sections of the cerebellar vermis from wild-type and SCA3 mice. GFP was diffusely expressed in all lobules of the wild-type mouse cerebellum with strong expression in lobule X (Fig. 4a, c, d). Interestingly, the expression was limited to PCs, most likely because of the nature of the MSCV promoter [8]. In contrast, only a trace of transgene expression was observed in most lobules of SCA3 mice except lobule X, where GFP was robustly expressed in PCs (Fig. 4b, e, f). A recent study has shown that ataxin-1 with abnormally expanded polyQ represses the transcription of vascular endothelial growth factor (VEGF) and causes a decrease in cerebellar microvessel density and total vessel length [22]. Therefore, a possible explanation that accounts for the reduced transgene expression in most lobules of the SCA3 mouse cerebellum may be poor vascularization in the cerebellar cortex. To verify this hypothesis, expression levels of VEGF mRNA and protein in wild-type and SCA3-mouse cerebellum were examined by quantitative RT-PCR and western blot analysis. The results showed that the expression levels of VEGF were significantly decreased in the SCA3-mouse cerebellum compared with wild-type control mice (Supplementary figure 3). These results suggest poor vascularization in the SCA3-mouse cerebellum.

Fig. 3 Defect in RORα expression in the nuclei of SCA3-mouse PCs. ▶ Cerebellar slices were triple-immunostained for mGluR1 (*green*), RORα (*magenta*), and calbindin (*blue*). **a** In a wild-type mouse, RORα was present in the nuclei of PCs (*arrows in right panels*) and interneurons, while mGluR1 was localized in the dendritic spines (*upper left and lower right panels*). **b** In the SCA3 mouse cerebellum, the nuclei of interneurons were clearly immunolabeled for RORα, whereas the PC soma (*arrows in right panels*) displayed no or very faint immunolabeling for RORα. mGluR1 was expressed in SCA3-mouse PC dendrites but formed larger clusters (*upper left and lower right panels*) compared to the fine clusters in the dendritic spines of wild-type-mouse PCs (*upper left and lower right panels* in **a**). *Scale bar*, 20 μm

Elimination of Mutant Ataxin-3 Aggregates in SCA3-Mouse PCs Expressing CRAG

We examined whether mutant ataxin-3 aggregates were eliminated by intravenously applied AAV9 expressing CRAG. The aggregates were visualized by immunostaining cerebellar slices for the HA tag on the N-terminus of mutant ataxin-3 [5]. The aggregates were found in almost all PCs in the non-injected SCA3 mouse cerebellum (Fig. 5a, lower panels). In sharp contrast, almost no aggregates were observed in lobule X of AAV9-treated SCA3 mice, where CRAG was robustly expressed (Fig. 5a, upper panels). The aggregates were not

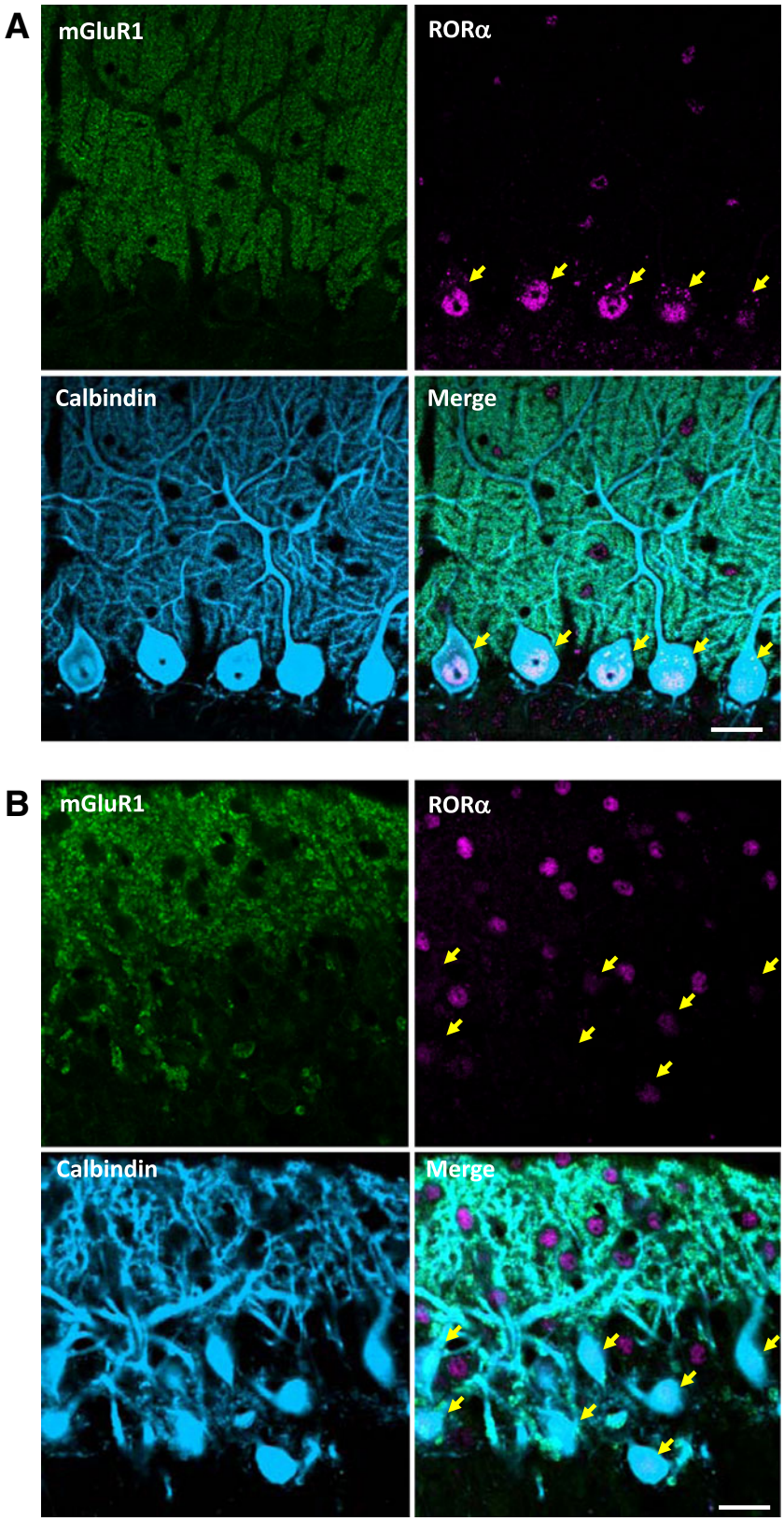

removed in non-transduced PCs in the neighboring lobules. We quantitatively assessed the CRAG-induced elimination of the aggregates by comparing the areas of aggregates in transduced lobule X with non-transduced lobule IX. The results

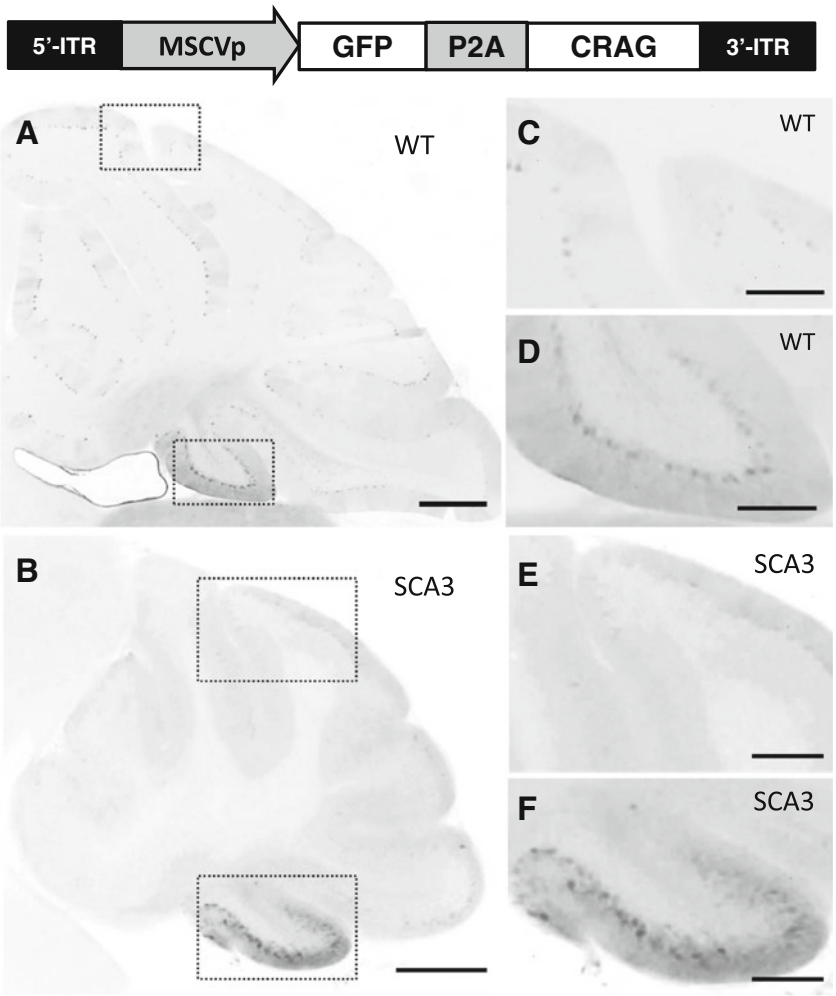

Fig. 4 Transduction of PCs by intravenously applied AAV9 expressing GFP and CRAG. Cerebellar slices were immunostained for GFP. **a**, **b** Cerebellum slices from an AAV9-injected wild-type mouse (**a**) and an AAV9-injected SCA3 mouse (**b**). **c**–**f** Magnified images of the areas surrounded by the *dotted lines* in **a** (**c**, **d**) and **b** (**e**, **f**). *Scale bar*, 500 μm (**a**, **b**); 200 μm (**c**–**f**)

showed a significant decrease in the number and size of the aggregates in the AAV9-infected and CRAG-expressing lobule X compared to non-transduced lobule IX (Fig. 5b). Moreover, CRAG-expressing PC soma were arranged in an orderly monolayer (arrows in Fig. 5a, upper panels) in contrast to the disrupted arrangement of PC soma in lobule X of the non-injected mouse cerebellum (arrows in Fig. 5a, lower panels).

Attenuation of Dendrite Development Defects in SCA3-Mouse PCs by the Induced Expression of CRAG

We next examined whether the impaired development of PC dendrites, which was observed in 14-week-old SCA3 mice, was inhibited or attenuated by the expression of recombinant CRAG. As shown in Fig. 1a, the membrane capacitance of SCA3-mouse PCs was significantly smaller than that of wild-type PCs. The AAV9-mediated expression of CRAG in mutant PCs significantly increased their membrane capacitance by 1.5-fold (Fig. 6a). There was a statistically significant difference in membrane capacitance between CRAG-expressing PCs (262.1±16.0 pF, $n=28$ PCs from four mice) and non-injected SCA3 mice (174.2±12.6 pF, $n=27$ PCs from four mice) (**$p<0.01$) or non-transduced PCs from AAV9-treated SCA3 mice (155.7±9.5 pF, $n=7$ PCs from three mice) (††$p<0.01$), suggesting that the impairment of dendritic differentiation in SCA3-mouse PCs had been attenuated by CRAG-mediated decrease in the amount of mutant ataxin-3. Indeed, immunostaining of biocytin infused through a patch pipette showed more elongated and arborized dendrites in SCA3-mouse PCs expressing CRAG when compared to neighboring, non-transduced PCs (Fig. 6b).

Presence of SSE in SCA3-Mouse PCs Overexpressing CRAG

We examined whether SCA3-mouse PCs expressing CRAG show SSE at the PF to PC synapses of SCA3 mice (Fig. 2a). The amplitudes of PF EPSCs in non-transduced PCs increased to approximately 140 % of the original amplitude in response to tetanic stimulation, indicating a complete defect in mGluR-mediated SSE. In contrast, the PF EPSC amplitude decreased drastically to approximately 30 % of prestimulation levels in CRAG-expressing PCs in the same animal (Fig. 7a), clearly

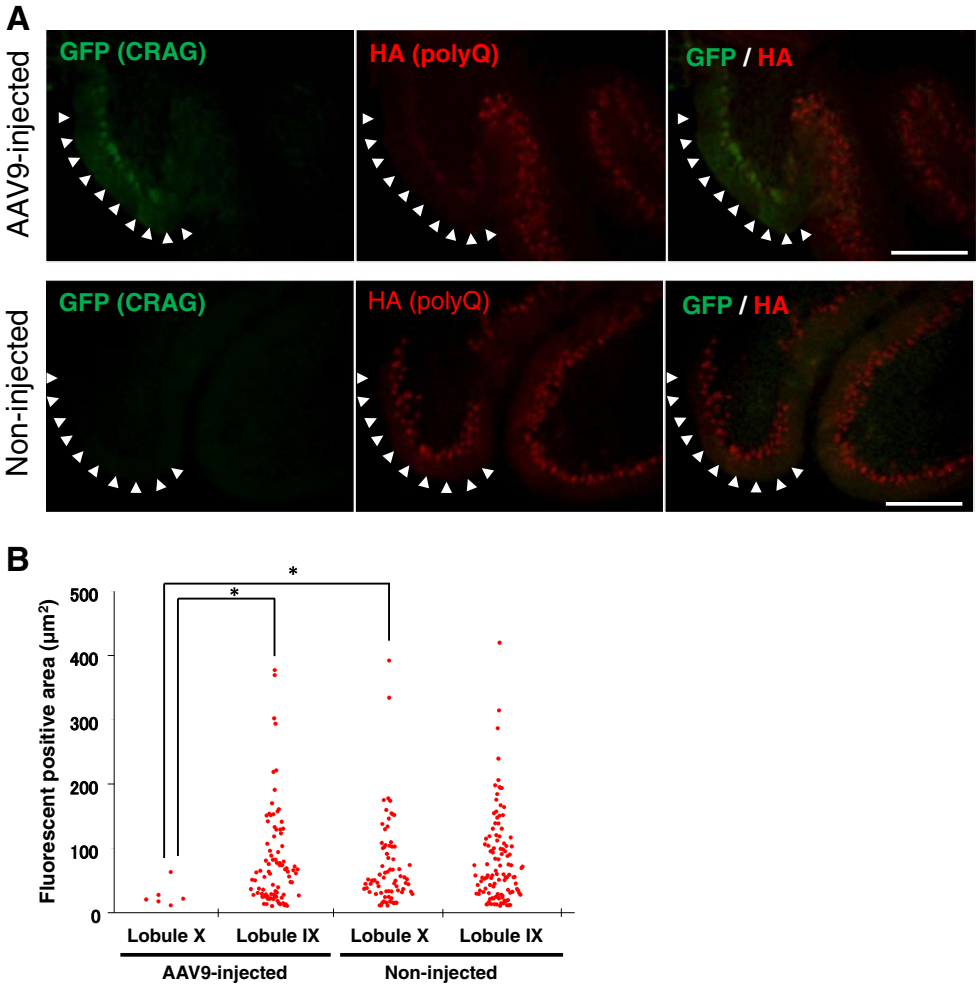

Fig. 5 Clearance of mutant ataxin-3 aggregates by AAV9-mediated expression of CRAG. **a** Cerebellar slices double-immunolabeled for GFP and HA-tagged mutant ataxin-3. GFP-expressing PCs simultaneously express recombinant CRAG. The *upper and lower panels* are slices from AA9-injected and non-injected SCA3 mice, respectively. *Arrowheads* indicate the transduced area in lobule X of an AAV9-injected SCA3 mouse (*upper panels*) and the corresponding region in a non-injected SCA3 mouse (*lower panels*). *Scale bar*, 200 μm. **b** Quantitative analysis of aggregates in transduced lobule X and nearly non-transduced lobule IX. The areas of aggregates immunolabeled for HA are plotted on the *graph*. *Asterisks* indicate a statistically significant difference as determined by the Mann–Whitney *U* test, $*p<0.05$

showing the existence of SSE, although the suppressed transmission recovered to the initial levels more quickly (approximately 20 s) compared to wild-type PCs (approximately 60 s) (Fig. 2a). There were significant differences in the percent change in PF

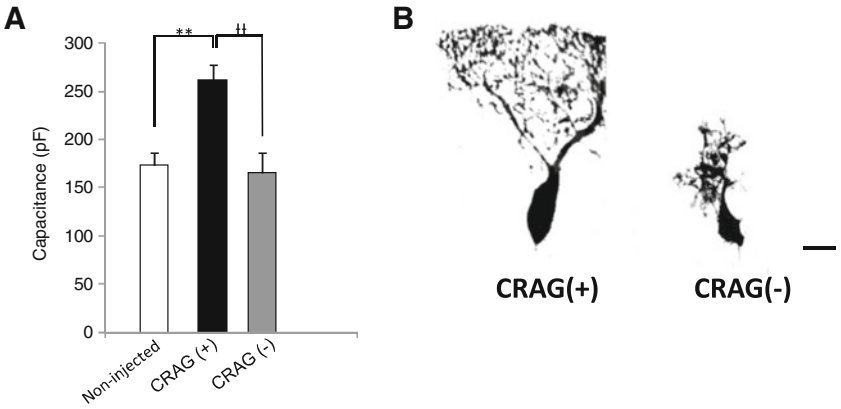

Fig. 6 Development of dendritic arborization in CRAG-expressing PCs from SCA3 mice. **a** Summary graph showing the averaged membrane capacitance of naïve PCs from non-injected SCA3 mice, recombinant CRAG-expressing PCs (*CRAG (+)*) and non-transduced PCs (*CRAG (−)*) from SCA3 mice. **b** Representative images of biocytin-immunolabeled PCs expressing recombinant CRAG (*CRAG (+)*) and non-transduced PCs (*CRAG (−)*) from an AAV9-treated SCA3 mouse. *Scale bar*, 20 μm. *Asterisks* and *daggers* indicate statistically significant differences as determined by one-way ANOVA followed by Tukey's post hoc test, $**p<0.01$, $††p<0.01$

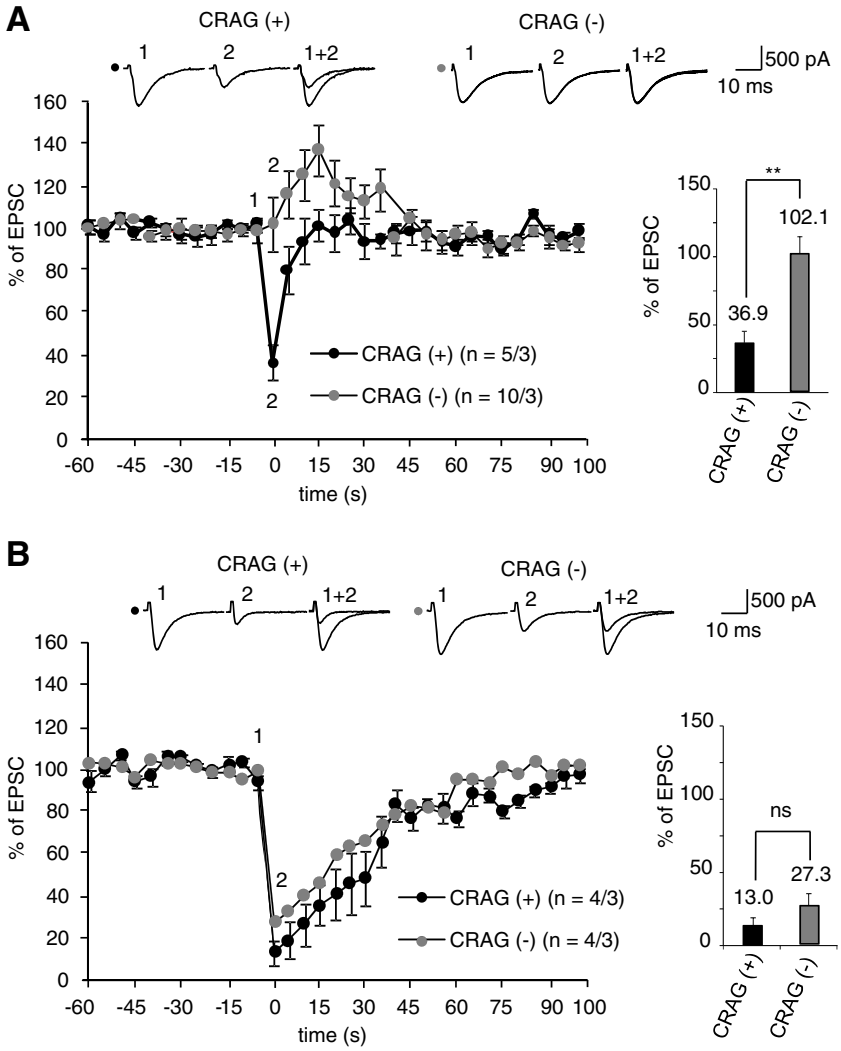

Fig. 7 Decrease in the amount of mutant ataxin-3 in SCA3-mouse PCs restored the mGluR-triggered SSE at PF–PC synapses. PF EPSCs were recorded from transduced PCs (*CRAG (+)*) and non-transduced PCs (*CRAG (−)*). **a** Time course of changes in the PF EPSC amplitude (*left*) and the percentage of the EPSC amplitude just after the burst stimulation relative to the baseline value (*right*), showing the restoration of the SSE in SCA3-mouse PCs expressing CRAG. **b** Time course of changes in the PF EPSC amplitude after a 5-s depolarization of PCs, showing the reliable occurrence of the DSE in wild-type and SCA3 mouse PCs. The *right graph* shows the percentage of the EPSC amplitude just after the depolarization. *Inset traces* in **a** and **b** represent the last EPSC of the basal recordings (the EPSC just before the stimulation) (*1*) and the first EPSC after the PF burst in each experimental condition (*2*). The numbers (*n*) of tested PCs and animals (PCs/animals) are indicated in the *graph*. *Asterisks* indicate a statistically significant difference in comparison to wild-type mice as determined by an unpaired *t* test, $^{**}p<0.01$

amplitude 5 s after tetanic stimulation between non-transduced PCs (102.1±12.7 %, $n=10$ cells from three animals) and CRAG-expressing PCs (36.9±8.3 %, $n=5$ cells from three animals) ($^{*}p<0.05$).

Again, DSE was observed in both CRAG-expressing and non-transduced PCs, and the reduction in PF amplitude did not significantly differ between the two groups (Fig. 7b, right graph) ($p=0.21$). These results suggest that, in addition to the impairment of dendritic development, the postnatal deposition of mutant ataxin-3 is responsible for the defect in mGluR signaling within SCA3-mouse PCs.

High-Frequency Firing in SCA3-Mouse PCs Expressing CRAG

A recent study using yeast artificial chromosome SCA3 Q84 transgenic mice in early stages (before morphological defects in PCs) showed aberrant, spontaneous firing in PCs such as burst firing and loss of repetitive firing; this is in contrast to the tonic and repetitive spontaneous firing observed in wild-type PCs [23]. We have previously shown that the frequency of action potentials in response to various amounts of current injection was consistently lower in SCA3 mice than in wild-type animals [5]. Although the firing profiles in transgenic mouse PCs likely differed depending on which transgene was expressed (full length or truncated) and their pathological stages (before or after the appearance of morphological alteration), these results suggest aberrant properties in the generation of action potentials in the PCs of SCA3 model mice expressing mutant ataxin-3 with abnormally expanded polyQ. We then examined whether a decrease in the amount of mutant ataxin-3 by CRAG expression could prevent SCA3-mouse PCs from decreasing the firing rate. In the current-clamp mode, a current injection into a cell generated action potentials in CRAG-expressing PCs and non-transduced PCs from AAV9-injected SCA3 mice and also PCs from non-injected mice (Fig. 8 inset traces). As we

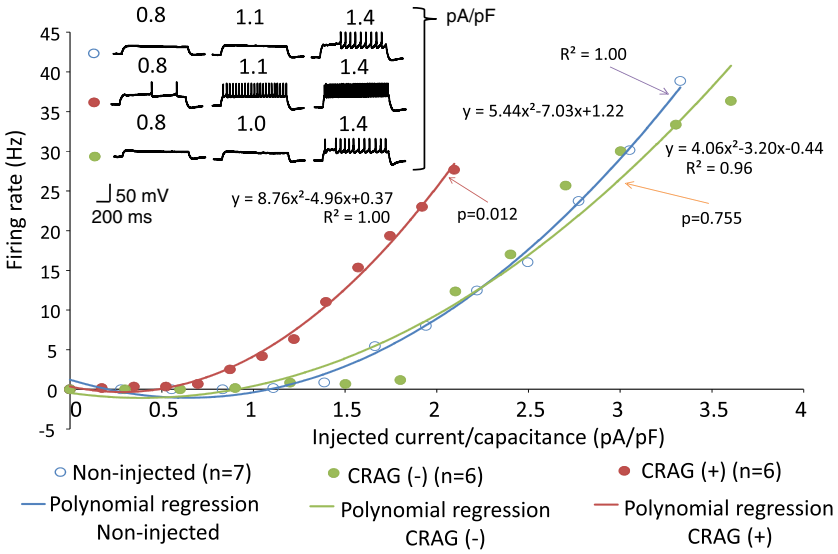

Fig. 8 Increased firing rates normalized to membrane capacitance (Cm) in recombinant CRAG-expressing PCs from AAV9-treated SCA3 mice. A depolarizing step current was applied to naïve PCs from non-injected SCA3 mice and to non-transduced PCs (*CRAG (−)*) and recombinant CRAG-expressing PCs (*CRAG (+)*) from SCA3 mice. The frequencies (in hertz) of the action potentials were plotted against the volume of injected currents (pA) per unit of Cm (pF). To compare the firing rates of these groups with different pA/pF ratios, we used a polynomial regression method. The quadratic function for each group is plotted near their function diagram. *R* is the coefficient of regression and shows the adequate accuracy of averaged data. There are statistically significant differences determined by one-way ANOVA followed by Tukey's post hoc test in the firing rates between recombinant CRAG-expressing PCs from AAV9-treated SCA3 mice and naïve PCs from non-injected SCA3 mice. *Insets* show representative traces of current injection-evoked repetitive action potentials recorded at similar pA/pF ratios

expected, the frequency of the action potentials (firing rate) to the injected current per unit of membrane capacitance was consistently higher in CRAG-expressing PCs compared to non-transduced PCs from AAV9-injected SCA3 mice and those from non-injected SCA3 mice (Fig. 8). There was a significant difference in the frequency of action potential generation between CRAG-expressing PCs from AAV9-injected mice and PCs from non-injected SCA3 mice ($p = 0.012$).

Discussion

Our patch-clamp analysis of cerebellar slices showed a significantly smaller Cm in PCs from SCA3 mice than in those from wild-type mice, suggesting a reduction in dendritic arborization in SCA3-mouse PCs that was confirmed by biocytin immunolabeling of recorded PCs. Moreover, in contrast to the overall preservation of AMPA receptor-mediated fast synaptic transmission, mGluR-triggered retrograde suppression of PF–PC synapses was almost completely abrogated in SCA3-mouse PCs. Postmortem brain examinations of SCA3 patients show marked neuronal loss primarily in pontine nuclei, dentate nucleus of the cerebellum, and the substantia nigra [24, 25]. PCs also show neurodegeneration but are relatively preserved [26]. A critical question is whether the preserved PCs are functionally intact or not. Our study clearly showed functional impairment of mGluR signaling in SCA3-mouse PCs, which could contribute to the ataxia observed in SCA3 patients.

Immunohistochemistry showed that mGluR1 protein was clearly expressed but aberrantly localized and aggregated in PC dendrites of SCA3 mice (Fig. 3). These findings are reminiscent of the spontaneously occurring classical *staggerer* mutant mice [27], which show severe ataxia with an atrophied cerebellum and a complete loss of mGluR-signaling and abnormally aggregated mGluR1 in their PCs [19] (Supplementary figure 2). The *staggerer* mouse is a loss-of-function mutant caused by a 122-bp deletion of the *rora* gene, which encodes the ligand-binding domain of the RORα protein [21]. RORα is a transcription factor that triggers the expression of various molecules including some involved in dendritic differentiation and glutamate signaling [20], and *staggerer* mice show a defect in RORα-mediated transcription. Interestingly, ataxin-1, the protein responsible for SCA type1 (SCA1), forms a transcriptional complex with RORα via Tip60. The abnormal expansion of the polyQ tract in ataxin-1 disrupts the binding of ataxin-1 with RORα, which results in the disruption of RORα-mediated gene transcription [20, 28]. Therefore, it is suggested that *staggerer* mutant mice and SCA1 patients share a similar pathology. Our present results showing a markedly decreased amount of RORα in the nuclei of SCA3-mouse PCs (Fig. 3) suggest that although the underlying mechanism remains to be defined, the abnormal phenotypes in the cerebellum and the resultant ataxia of SCA3 mice are likely caused by a disruption of RORα-mediated transcription.

However, it is possible that the transgene insertion and resultant gene disruption caused observed defects in our SCA3 mouse line. To exclude this possibility, we tried to reduce the amount of mutant ataxin-3 in postnatal SCA3 mouse PCs. For this purpose, we used AAV9 because its intravenous administration allows us to deliver a transgene into the CNS [29–31]. Fourteen weeks after the AAV9 injection, CRAG was diffusely expressed in whole cerebellar lobules of wild-type animals, whereas it was largely limited to lobule X in the SCA3 cerebellum (Fig. 4). In regard to defects of transgene expression in other lobules of the SCA3 mouse cerebellum, we hypothesized poor vascularization in the cerebellar cortex of SCA3 mice because ataxin-1 with abnormally expanded polyQ repressed the transcription of VEGF and caused a decrease in cerebellar microvessel density and total vessel length [22]. The quantitative RT-PCR and western blot analysis confirmed significantly reduced expression levels of VEGF in the SCA3-mouse cerebellum (Supplementary figure 3), suggesting poor vascularization of the SCA3-mouse cerebellum. High expression levels of the transgene in lobule X of both the wild-type and mutant cerebellum are thought to be due to seepage of the cerebrospinal fluid (CSF) containing AAV9 from the choroid plexus of the fourth ventricle. Lobule X is close to the choroid plexus and in the path of CSF flow, which allows secreted AAV9 particles easy access to PCs. Although neonatal intravenous administration of AAV9 transduced only a limited area in the cerebellum, the efficient transduction of PCs in lobule X suggests that AAV delivery via the CSF flow, i.e., intrathecal administration of AAV9, could be a better alternative for transduction of brain tissue broadly.

AAV9-mediated expression of CRAG in SCA3-mouse PCs significantly prevented the accumulation of mutant ataxin-3 aggregates (Fig. 5), leading to improved dendritic differentiation, expression of SSE upon mGluR1 activation, and a more efficient spike generation in response to current injection (Figs. 6, 7, and 8). These results confirm that the postnatal deposition of mutant ataxin-3 with abnormally expanded polyQ in PCs in vivo disrupts dendritic development and mGluR signaling at PF–PC synapses.

Conclusions

We characterized advanced-stage SCA3 mice, which express truncated ataxin-3 with abnormally expanded CAG repeats in PCs and exhibit severe ataxia. Electrophysiological examination of SCA3-mouse PCs revealed a significant reduction in the Cm, a loss of synaptically evoked mGluR-mediated suppression of excitation at PF–PC synapses and impaired generation of action potentials upon current injection. Immunohistochemistry showed poor dendritic arborization and a marked decrease in the amount of nuclear RORα in PCs. A postnatal decrease in the amount of mutant ataxin-3 through AAV9-mediated CRAG expression prevented PCs from progressing to severe aberrant phenotypes.

Acknowledgments The authors are very grateful to Noriyuki Koibuchi for providing us with *staggerer* mutant mice. The authors would like to thank Dr. Andrey N. Shuvaev from the Institute of Undergraduate Core Programs, Siberian Federal University for his advice on our statistical analysis. This work was supported in part by the Funding Program for Next Generation World-Leading Researchers (LS021) to H. H and JSPS KAKENHI grant number 24700394 to A. K.

Conflict of Interest All authors state that there are no actual or potential conflicts of interest concerning the work presented in this manuscript.

References

1. Zoghbi HY, Orr HT. Glutamine repeats and neurodegeneration. Annu Rev Neurosci. 2000;23:217–47.
2. Kawaguchi Y, Okamoto T, Taniwaki M, Aizawa M, Inoue M, Katayama S, et al. CAG expansions in a novel gene for Machado-Joseph disease at chromosome 14q32.1. Nat Genet. 1994;8:221–8.
3. Torashima T, Koyama C, Iizuka A, Mitsumura K, Takayama K, Yanagi S, et al. Lentivector-mediated rescue from cerebellar ataxia in a mouse model of spinocerebellar ataxia. EMBO Rep. 2008;9:393–9.
4. Qin Q, Inatome R, Hotta A, Kojima M, Yamamura H, Hirai H, et al. A novel GTPase, CRAG, mediates promyelocytic leukemia protein-associated nuclear body formation and degradation of expanded polyglutamine protein. J Cell Biol. 2006;172:497–504.
5. Oue M, Mitsumura K, Torashima T, Koyama C, Yamaguchi H, Furuya N, et al. Characterization of mutant mice that express polyglutamine in cerebellar Purkinje cells. Brain Res. 2009;1255:9–17.
6. Iizuka A, Takayama K, Torashima T, Yamasaki M, Koyama C, Mitsumura K, et al. Lentiviral vector-mediated rescue of motor behavior in spontaneously occurring hereditary ataxic mice. Neurobiol Dis. 2009;35:457–65.
7. Torashima T, Iizuka A, Horiuchi H, Mitsumura K, Yamasaki M, Koyama C, et al. Rescue of abnormal phenotypes in δ2 glutamate receptor-deficient mice by the extracellular N-terminal and intracellular C-terminal domains of the δ2 glutamate receptor. Eur J Neurosci. 2009;30:355–65.
8. Takayama K, Torashima T, Horiuchi H, Hirai H. Purkinje-cell-preferential transduction by lentiviral vectors with the murine stem cell virus promoter. Neurosci Lett. 2008;443:7–11.
9. Tamayose K, Hirai Y, Shimada T. A new strategy for large-scale preparation of high-titer recombinant adeno-associated virus vectors by using packaging cell lines and sulfonated cellulose column chromatography. Hum Gene Ther. 1996;7:507–13.
10. Miyake K, Miyake N, Yamazaki Y, Shimada T, Hirai Y. Serotype-independent method of recombinant adeno-associated virus (AAV) vector production and purification. J Nippon Med Sch. 2012;79:394–402.
11. Maejima T, Hashimoto K, Yoshida T, Aiba A, Kano M. Presynaptic inhibition caused by retrograde signal from metabotropic glutamate to cannabinoid receptors. Neuron. 2001;31:463–75.
12. Brown SP, Brenowitz SD, Regehr WG. Brief presynaptic bursts evoke synapse-specific retrograde inhibition mediated by endogenous cannabinoids. Nat Neurosci. 2003;6:1048–57.
13. Marcaggi P, Attwell D. Endocannabinoid signaling depends on the spatial pattern of synapse activation. Nat Neurosci. 2005;8:776–81.

14. Marcaggi P, Attwell D. Short- and long-term depression of rat cerebellar parallel fibre synaptic transmission mediated by synaptic crosstalk. J Physiol. 2007;578:545–50.
15. Safo P, Cravatt B, Regehr W. Retrograde endocannabinoid signaling in the cerebellar cortex. Cerebellum. 2006;5:134–45.
16. Hashimotodani Y, Ohno-Shosaku T, Kano M. Ca2+-assisted receptor-driven endocannabinoid release: mechanisms that associate presynaptic and postsynaptic activities. Curr Opin Neurobiol. 2007;17:360–5.
17. Kano M, Ohno-Shosaku T, Hashimotodani Y, Uchigashima M, Watanabe M. Endocannabinoid-mediated control of synaptic transmission. Physiol Rev. 2009;89:309–80.
18. Best AR, Regehr WG. Identification of the synthetic pathway producing the endocannabinoid that mediates the bulk of retrograde signaling in the brain. Neuron. 2010;65:291–2.
19. Mitsumura K, Hosoi N, Furuya N, Hirai H. Disruption of metabotropic glutamate receptor signalling is a major defect at cerebellar parallel fibre–Purkinje cell synapses in staggerer mutant mice. J Physiol. 2011;589:3191–209.
20. Serra HG, Duvick L, Zu T, Carlson K, Stevens S, Jorgensen N, et al. ROR[alpha]-mediated Purkinje cell development determines disease severity in adult SCA1 mice. Cell. 2006;127:697–708.
21. Hamilton BA, Frankel WN, Kerrebrock AW, Hawkins TL, Fitzhugh W, Kusumi K, et al. Disruption of the nuclear hormone-receptor ROR-alpha in staggerer mice. Nature. 1996;379:736–9.
22. Cvetanovic M, Patel JM, Marti HH, Kini AR, Opal P. Vascular endothelial growth factor ameliorates the ataxic phenotype in a mouse model of spinocerebellar ataxia type 1. Nat Med. 2011;17:1445–7.
23. Shakkottai VG, do Carmo Costa M, Dell'Orco JM, Sankaranarayanan A, Wulff H, Paulson HL. Early changes in cerebellar physiology accompany motor dysfunction in the polyglutamine disease spinocerebellar ataxia type 3. J Neurosci. 2011;31:13002–14.
24. Bezprozvanny I, Klockgether T. Therapeutic prospects for spinocerebellar ataxia type 2 and 3. Drugs Future. 2010;34:991–9.
25. Stevanin G, Duerr A, Brice A. Clinical and molecular advances in autosomal dominant cerebellar ataxias: from genotype to phenotype and physiopathology. Eur J Hum Genet: EJHG. 2000;8:4.
26. Seidel K, Siswanto S, Brunt EP, Dunnen W, Korf H-W, Rüb U. Brain pathology of spinocerebellar ataxias. Acta Neuropathol. 2012;124:1–21.
27. Sidman RL, Lane PW, Dickie MM. Staggerer, a new mutation in the mouse affecting the cerebellum. Science. 1962;137:610–2.
28. Albert RLS. Neurodegeneration: a case of arrested development? Cell. 2006;127:669–71.
29. Foust KD, Nurre E, Montgomery CL, Hernandez A, Chan CM, Kaspar BK. Intravascular AAV9 preferentially targets neonatal neurons and adult astrocytes. Nat Biotech. 2009;27:59–65.
30. Gray SJ, Matagne V, Bachaboina L, Yadav S, Ojeda SR, Samulski RJ. Preclinical differences of intravascular AAV9 delivery to neurons and glia: a comparative study of adult mice and nonhuman primates. Mol Ther. 2011;19:1058–69.
31. Miyake N, Miyake K, Yamamoto M, Hirai Y, Shimada T. Global gene transfer into the CNS across the BBB after neonatal systemic delivery of single-stranded AAV vectors. Brain Res. 2011;1389:19–26.